THE JOURNAL OF PHYSICAL CHEMISTRY C

Article

pubs.acs.org/JPCC

Structure and Basicity of Microporous Titanosilicate ETS-10 and Vanadium-Containing ETS-10

Meiling Guo,[†,‡] Evgeny A. Pidko,[§] Fengtao Fan,[†] Zhaochi Feng,[†] Jan P. Hofmann,[⊥] Bert M. Weckhuysen,[⊥] Emiel J. M. Hensen,*[,§] and Can Li*[,†]

[†]State Key Laboratory of Catalysis, Dalian Institute of Chemical Physics, Chinese Academy of Sciences, 457 Zhongshan Road, Dalian, 116023, China

[‡]Graduate University of Chinese Academy of Sciences, 457 Zhongshan Road, Dalian, 116023, China

[§]Inorganic Materials Chemistry, Schuit Institute of Catalysis, Eindhoven University of Technology, P.O. Box 513, 5600 MB Eindhoven, The Netherlands

[⊥]Inorganic Chemistry and Catalysis, Debye Institute for NanoMaterials Science, Utrecht University, Universiteitsweg 99, 3584 CG Utrecht, The Netherlands

Supporting Information

ABSTRACT: ETS-10 has attracted considerable attention as a base catalyst. It is desirable to confirm the location of basic sites. Vanadium-substituted ETS-10 also attracts much attention for the interesting feature that the Ti can be fully replaced by V without changing its topology. It is important to characterize the local environment upon V substitution for understanding the property and reactivity of ETVS-10. The structural and acid−base properties of pure titanosilicate ETS-10 and a series of vanadium-substituted ETVS-10 with different framework V content were studied by a combination of Raman spectroscopy and FTIR of absorbed acetylene and carbon monoxide as molecular probes. The substitution of up to 70% of Ti atoms with V in the structure of ETS-10 results in ETVS-10 materials with a homogeneous distribution of Ti and V species. At higher V concentrations, a distinct phase separation between the vanadium-rich domains is observed. The intrinsic basicity of ETVS-10 as revealed by FTIR spectroscopy of adsorbed C_2H_2 gradually increases with the increasing V content. It is shown that the specific basicity of the ETS-10 lattice is mainly associated with the presence of highly basic oxygen centers adjacent to the lattice defects. Liquid phase Knoevenagel condensation of benzaldehyde with ethyl cyanoacetate was used as a test reaction to investigate the catalytic reactivity of different basic sites in the synthesized materials. The reactivity of the materials considered in the base-catalyzed Knoevenagel condensation is determined not only by the strength of the basic sites but also by their density. The optimum combination of both factors is achieved for the ETVS-10 material with V/(Ti+V) ratio of 70%.

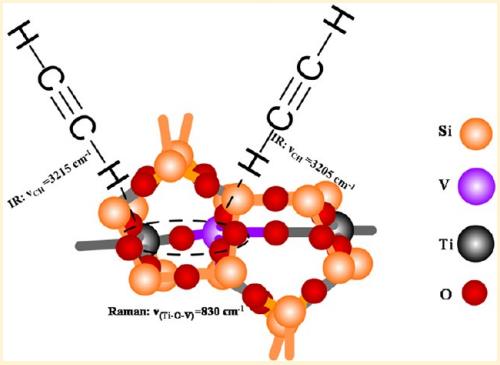

1. INTRODUCTION

The microporous titanosilicate ETS-10 is a base catalyst that has been used in the dehydration of *tert*-butyl alcohol,[1−3] the dehydrogenation of alcohols such as ethanol, 2-propanol, and cyclohexanol,[3,4] the aldol condensation of acetone,[5,6] and the isomerization of glucose.[7] Compared to the well-understood Brønsted acidity in zeolites,[8] the nature and reactivity of basic sites in these materials remain a subject of debate. In ETS-10, one identifies octahedral Ti^{4+} ions besides tetrahedral framework Si^{4+} ions.[9] Each $[TiO_6]$ lattice unit bears two negative charges, which are usually balanced by exchangeable Na^+ and K^+ ions.

Adsorption of small probe molecules in combination with vibrational spectroscopy is a widely used technique to study the acid−base properties of active sites in heterogeneous catalysts.[10−12] Acetylene has been used for estimating the strength of basic sites by FTIR spectroscopy. Upon adsorption, the rather acidic CH moiety of C_2H_2 forms weak hydrogen bonds with basic lattice oxygen sites. In addition, the electron-rich π-system of acetylene can interact with Lewis acidic cations. As a result the properties of the molecular probe interacting with the basic sites can be substantially influenced by the interaction with the neighboring Lewis acid. Co-adsorption of two different probe molecules, one of which is able to selectively bind with the latter sites, represents a potential route for analysis of the intrinsic basicity of heterogeneous catalysts.[12] CO is such a probe molecule that can be used to selectively characterize the Lewis acidic alkali cations in zeolites.[13,14] Thus, by coadsorbing CO and acetylene,

Received: June 6, 2012
Revised: July 24, 2012
Published: July 24, 2012

it seems plausible to separately probe Lewis acidic and basic sites.

The chemical properties of ETS-10 can be adjusted not only by varying the extraframework cationic species, but also by substituting some of the lattice Ti and Si atoms by other transition metals.[3,15−23] For example, vanadium-substituted ETS-10 (ETVS-10) have attracted much attention because of their interesting chemical properties and potential application as photocatalysts.[16,19−23] An attractive feature of V-substituted ETS-10 is the possibility to widely vary the ratio between Ti and V atoms in the framework without changing its topology. In the absence of Ti, the vanadosilicate AM-6 is obtained, which is isostructural to ETS-10.[24]

It is desirable to identify the location of the basic sites and the interaction of Lewis acidic and basic sites of ETS-10. It is also very important to characterize the changes in the local environment and basicity upon the V substitution. In this contribution, the basic properties of ETS-10 were studied by FTIR spectroscopy of absorbed acetylene and carbon monoxide, complemented by DFT calculation. The distribution of Ti and V atoms in ETVS-10 materials is analyzed by Raman microspectroscopy. The base-catalyzed liquid phase Knoevenagel condensation of benzaldehyde with ethyl cyanoacetate was used as a test reaction to evaluate the catalytic reactivity of basic sites in different ETVS-10.

2. EXPERIMENTAL SECTION

Synthesis. A typical synthesis of ETVS-10 was performed as follows. Mixture A was prepared by mixing 5.8 mL of sodium silicate solution (20 wt % SiO_2, 6.9 wt % Na_2O), NaOH (1.69 g), and K_2SO_4 (1.6 g) in 10 mL of deionized water with stirring for 30 min. Concentrated H_2SO_4 (0.66 mL) was added to [Ti(iPrO)$_4$] with stirring for 5 min, followed by addition of 15 mL of deionized water. This mixture was boiled for 10 min to obtain anatase nanoparticles used as the titanium source. Subsequently, a vanadate solution ($VOSO_4$) was slowly added to the solution containing the anatase nanoparticles in a dropwise manner to obtain mixture B. The molar ratio of (V+Ti)/Si is 5.02 for a series of ETVS-10 with different V content. The two mixtures A and B were then mixed under stirring for 30 min to obtain the final gel. For the synthesis of ETVS-10 with V contents of 0.9 and 1.0, a small amount of ETS-10 (10 mg) was added to the gel as seeds for crystallization. Finally, the gel was transferred into a Teflon-lined stainless steel autoclave and placed in an oven for 12 h at 230 °C. The sample was filtered and washed with deionized water and dried overnight at 80 °C. The following notation is used to differentiate the ETVS-10 materials investigated in this work: ETVS-10(x), where x corresponds to the V/(V+Ti) molar ratio in the initial gel.

Characterization. XRD patterns were recorded on a Rigaku D/Max-2500/PC powder diffractometer. Each sample powder was scanned by using Cu Kα radiation with an operating voltage of 40 kV and an operating current of 200 mA. 2θ angles from 5° to 40° were measured with the speed of 5 deg/min. The catalysts were ground and pressed in sample holders for measurements. The morphology of the synthesized samples was examined with use of Scanning Electron Microscopy (SEM). SEM images were collected with a QUANTA 200F electron microscope. Visible Raman spectra were collected on a homemade Raman spectrograph system. The scattered light was collected by the ellipse collecting mirror in a backscattering geometry and focused into the entrance of the Raman spectrograph. The Raman spectra were collected with a spectral resolution of 2 cm^{-1} with the laser excitation at 532 nm from semiconductor lasers. Raman microspectroscopy imaging was carried out on a Renishaw inVia Raman microscope at 100× magnification, using StreamLine mode at 514 nm Ar ion laser excitation. For imaging, characteristic Raman bands have been selected and their intensity was mapped according to the band height. FTIR spectra were recorded with a Bruker Vertex V70 FTIR spectrometer in transmission mode. Typically, an about 10-mg sample was pressed into a self-supporting wafer and placed in a controlled-environment transmission cell. Prior to recording the spectra, the samples were dehydrated in vacuum at 300 °C (ramp 5 deg/min). After an isothermal period of 2 h at 300 °C the sample was cooled to room temperature in a vacuum. The spectra of adsorbed acetylene were recorded at room temperature and at different equilibrium pressures. The spectra of adsorbed CO were collected at −150 °C. After that, acetylene was introduced to the cell, and the spectra of adsorbed CO and acetylene were collected at −150 °C.

DFT Calculations. A 21T cluster (102 atoms) was used to model the sample−acetylene complexes (Figure S1, Supporting Information). Different possible adsorption sites of ETS-10 were compared. Dangling Si−O bonds of the model were saturated by H atoms located 1.4 Å from each terminal Si atom. Ti defect sites were modeled as Ti−OH at the periphery of the cluster. Full geometry optimization was performed for the cluster model and acetylene with the exception that the positions of boundary H were fixed according to their initial coordinates. Calculations were performed at the M06L/6-31G(d,p) level of theory, using Gaussian 09 program. Vibrational frequencies were computed analytically from the normal-mode analysis involving all atoms of the model in the harmonic approximation.

Basicity Tests. Liquid phase Knoevenagel condensation was used to test the basicity of the ETVS-10. The reactions were carried out in a 25 mL round-bottomed flask equipped with a Dimroth condenser. The reaction mixture was continuously stirred with a magnetic stirrer. Quantitative analyses of the products were performed on a gas chromatograph. For the reaction, 5 mmol of benzaldehyde (BA) and 5 mmol of ethyl cyanoacetate (ECA) were mixed with 7.5 mL of ethanol and 2.5 mmol of n-decane as the internal standard. After mixing 30 mg of catalyst to this solution, the suspension was heated to 60 °C for 1 h. The product was ethyl α-cyanocinnamate (ECC) as determined by GC-FID.

3. RESULTS AND DISCUSSION

Acid−Base Property of ETS-10. FTIR spectroscopy was used to investigate the basic properties of ETS-10 with acetylene as molecular probe (Figure 1). Adsorption of C_2H_2 on ETS-10 leads to the formation of two bands at 3212 and 3229 cm^{-1}, denoted as LF (low frequency) and HF (high frequency), respectively. These bands correspond to the ν_3 stretching vibrations of adsorbed acetylene. Because the relative intensities of these bands change independently with increasing C_2H_2 pressure, we assign them to acetylene molecules adsorbed on different sites of ETS-10. The strong perturbation of adsorbed C_2H_2 is apparent from the strong red shifts of the ν_3 stretching frequency compared to the gas phase (−58 and −75 cm^{-1}, respectively, for the HF and LF bands). Since the LF feature dominates at lower pressures, it can be assigned to the sites of stronger acetylene adsorption. With increasing

dx.doi.org/10.1021/jp305543m | J. Phys. Chem. C 2012, 116, 17124−17133

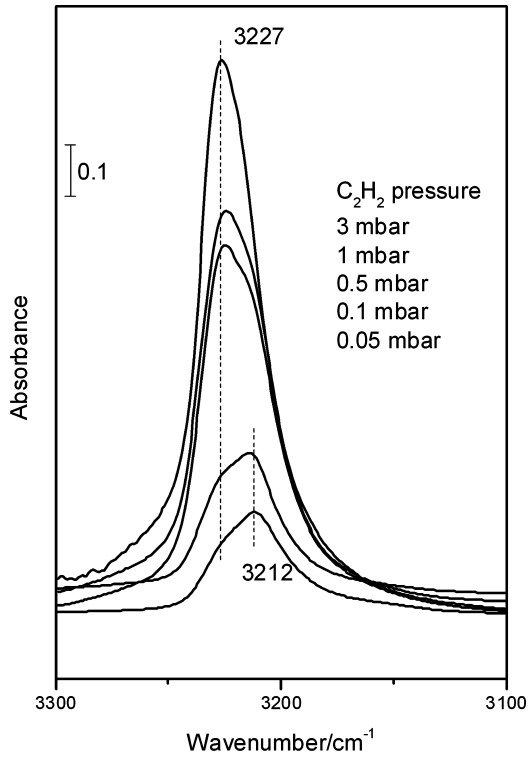

Figure 1. FTIR spectra of acetylene on ETS-10.

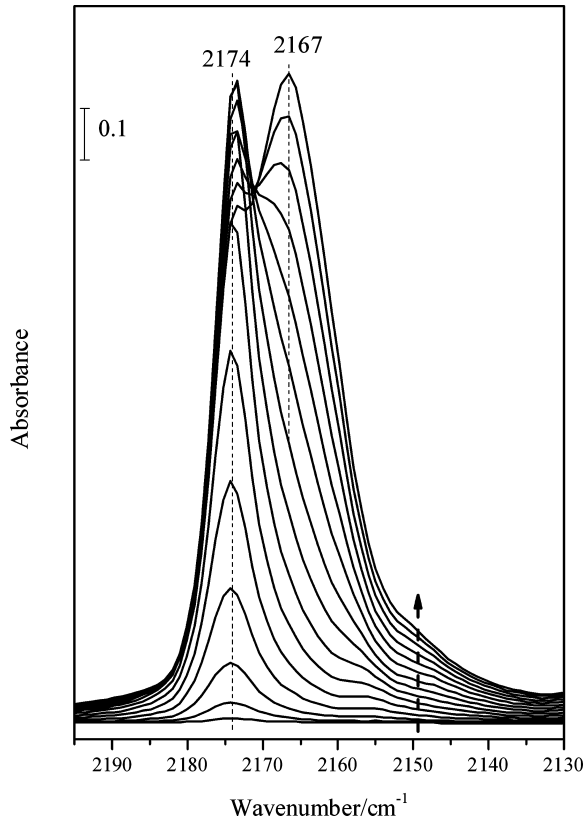

Figure 2. FTIR spectra of CO adsorbed on ETS-10. The dotted arrow indicates an increase in gas-phase equilibrium pressure of CO.

acetylene pressure, the sites associated with the LF band become saturated, whereas those characterized by the HF feature are still being populated.

For comparison, adsorption of acetylene to zeolite NaY was also investigated (Figure S2 Supporting Information). The smaller red shift for the HF and shoulder LF features observed evidence the weaker basicity of NaY zeolite compared to ETS-10. A similar conclusion was drawn by Tatsumi et al. with use of pyrrole as a probe.[25] For NaY, the HF band at 3245 cm^{-1} has been ascribed to the CH vibration of an acetylene π-complex (the interaction between C≡C of acetylene and Na^+ ions), and the LF band at 3215 cm^{-1} to the H-bonded species.[10]

In view of the similarity of the spectra for Na−Y and ETVS-10, the HF and LF bands of ETVS-10 can be assigned to the same adsorption modes. To further validate this interpretation, the interaction between ETS-10 and acetylene was studied by model DFT calculations. Ten different starting structures for C_2H_2 adsorption complexes at different sites of a cluster model of ETS-10 were constructed. Their geometry optimization resulted in three distinct configurations, namely, adsorption of acetylene on the Si−O−Si moieties (H-bonded species), on Na^+ extraframework cations (π-complex), and the framework oxygen atom (H-bonded species) adjacent to the Ti−OH defects as shown in Scheme 1. Adsorption to the Si−O−Si fragment gives the weakest complex (24 kJ/mol), which is characterized by a very small red shift of the asymmetric CH stretching (−10 cm^{-1}). Most of the initial adsorption configurations lead upon geometry optimization to π-complexes with extraframework Na^+ ions. These sites should thus be the dominant adsorption sites for C_2H_2. The adsorption energy is 46 kJ/mol and the red shift of ν_{CH} is −35 cm^{-1}. The red shift is independent of the local surrounding of the extraframework Na^+ ions. Adsorption to the basic oxygen sites adjacent to the defect Ti−OH fragments leads to the most pronounced perturbation of C_2H_2. The adsorption energy (33

Scheme 1. Acetylene Adsorption on (a) Si−O−Si Moieties, (b) Na^+ Extraframework Cations, and (c) Oxygen Adjacent to the Ti−OH Defect Site

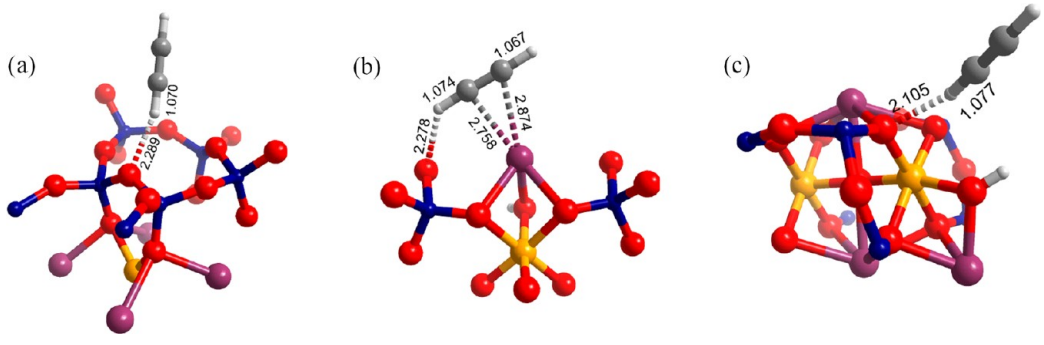

dx.doi.org/10.1021/jp305543m | J. Phys. Chem. C 2012, 116, 17124−17133

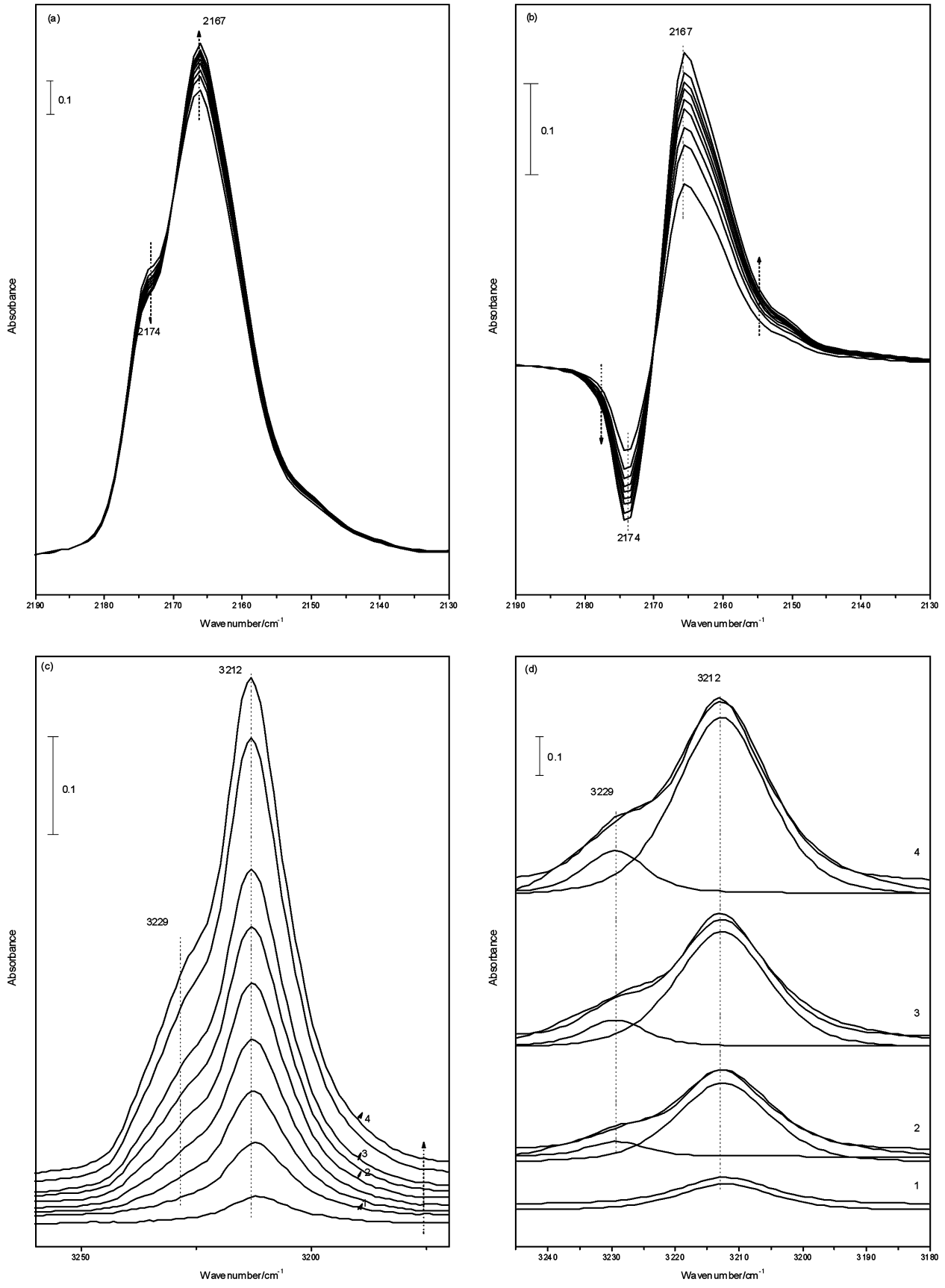

Figure 3. (a) FTIR spectra of CO along with the subsequent adsorption of acetylene to CO on ETS-10, (b) spectral changes in the CO region of part a, (c) FTIR spectra of acetylene along with the subsequent adsorption of acetylene to CO on the ETS-10, and (d) the deconvolution of 1, 2, 3, and 4 in part c.

dx.doi.org/10.1021/jp305543m | J. Phys. Chem. C 2012, 116, 17124−17133

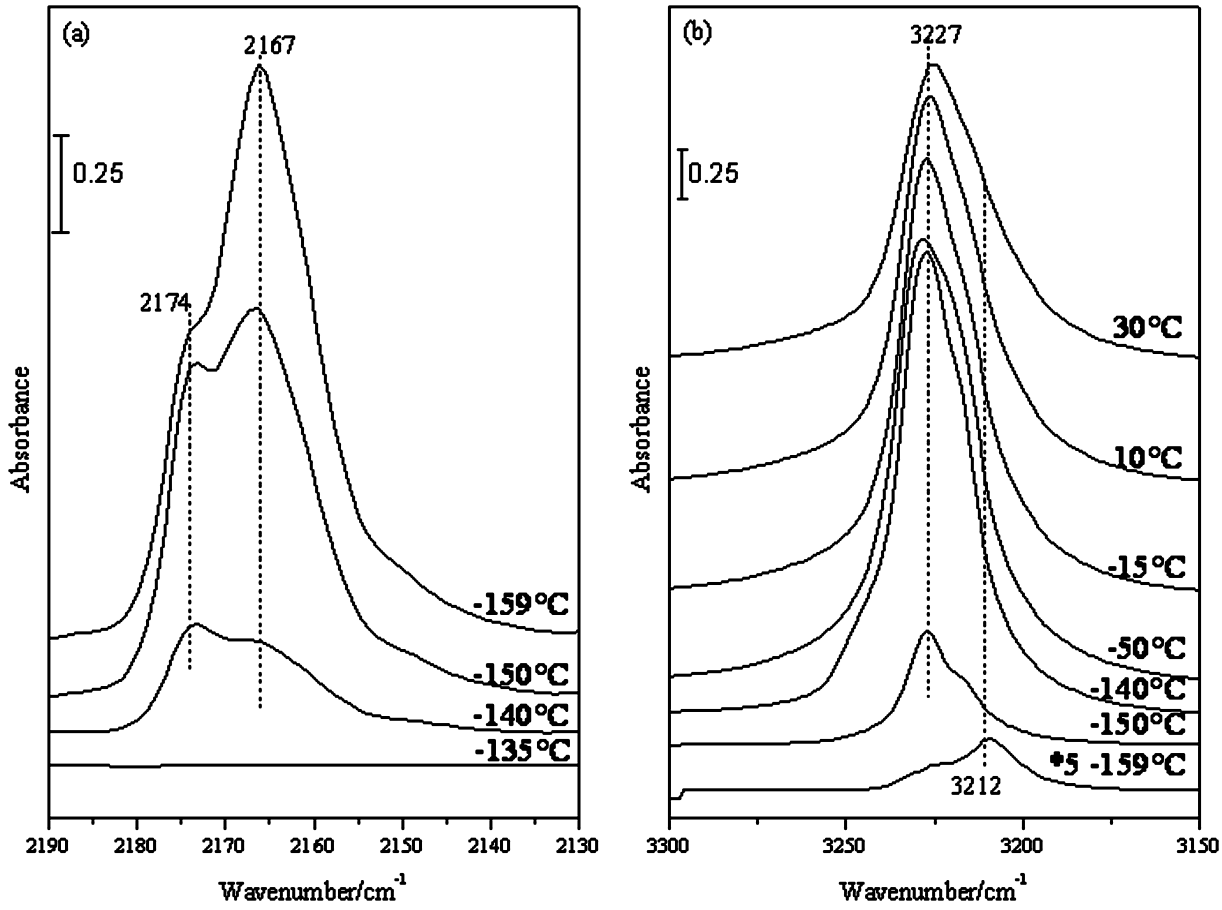

Figure 4. FTIR spectra of (a) CO and (b) acetylene adsorbed to ETS-10 as a function of temperature.

Table 1. Composition of ETVS-10 Samples

sample	ETS-10	ETVS-10(0.1)	ETVS-10(0.3)	ETVS-10(0.5)	ETVS-10(0.7)	ETVS-10(0.9)	AM-6
V/(V+Ti)	0	0.08	0.21	0.39	0.57	0.78	0.97
K/(K+Na)	0.22	0.34	0.13	0.20	0.11	0.16	0.16

kJ/mol) is close to that estimated for the case of adsorption to Na^+ ions. The red shift in this case is −73 cm^{-1}. The computational results confirm the assignments for HF and LF to the π-complex and the H-bonded species, respectively. The Na^+ ions act as Lewis acid centers and the framework oxygen atoms adjacent to the defect Ti−OH as basic centers.

To further detail the basic properties of these materials, the strengths of Lewis acidic extraframework cations and basic lattice sites were probed independently by monitoring the coadsorption of CO and C_2H_2, using infrared spectroscopy. These experiments were carried out at −150 °C. Figure 2 shows the IR spectra of CO adsorbed on ETS-10 with increasing CO coverage. At low pressures a single band is observed at 2174 cm^{-1} (denoted as CO-1), which corresponds

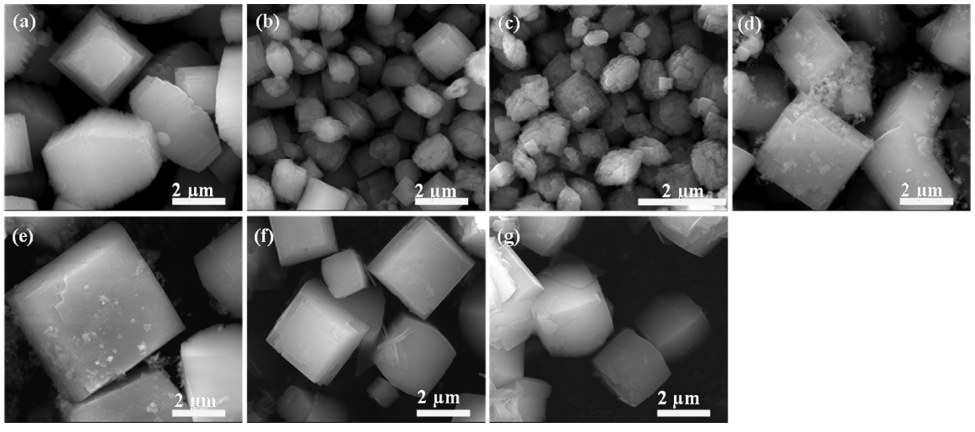

Figure 5. SEM images of (a) ETS-10, (b) ETVS-10(0.1), (c) ETVS-10(0.3), (d) ETVS-10(0.5), (e) ETVS-10(0.7), (f) ETVS-10(0.9), and (g) AM-6 samples.

dx.doi.org/10.1021/jp305543m | J. Phys. Chem. C 2012, 116, 17124−17133

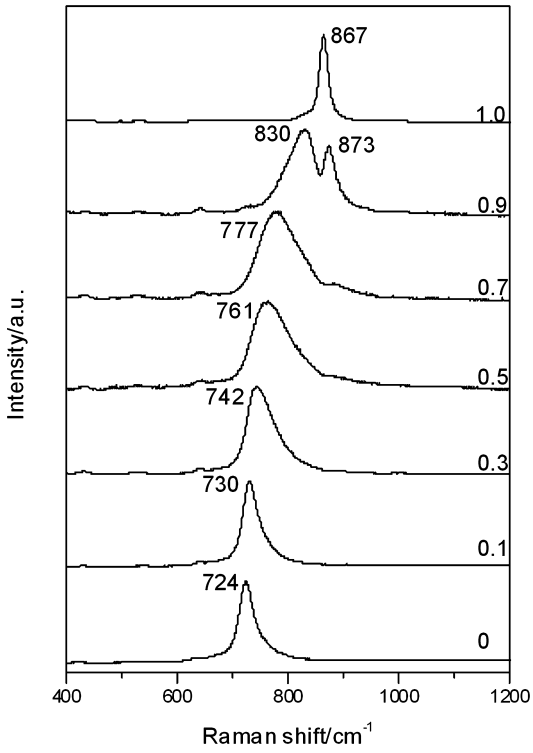

Figure 6. Raman spectra of ETVS-10 with different V content.

Scheme 2. The Relation of the Length of Ti-Rich and the Number of Ti−O−V Junctions along the Wire As a Function of V Content

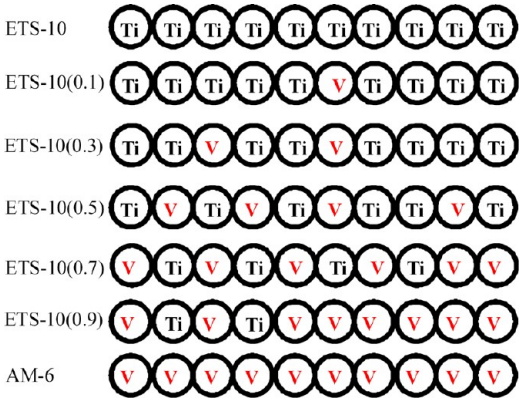

to CO adsorbed to Na^+ and K^+ ions.[26] In agreement with the literature,[26] it is seen that the increase of the CO coverage leads to a decrease of the band intensity at 2174 cm^{-1} and a concomitant increase of the band intensity at 2167 cm^{-1} (denoted as CO-2). The occurrence of an isosbestic point implies that these two bands are related to the common adsorption site. The band at lower wavenumber is due to multiple CO adsorptions to the exchangeable alkali cations.[26]

Subsequent introduction of acetylene to ETS-10 with adsorbed CO leads to minor changes of the CO stretching modes (Figure 3a,b). The intensity of CO-2 increases slightly, while the CO-1 intensity decreases with increasing C_2H_2 coverage. The corresponding changes in the CH stretching region are shown in panels c and d of Figure 3. At very low C_2H_2 pressure, only the LF band is observed (Figure 3d, 1). With increasing acetylene pressure, a distinct shoulder at higher frequencies (HF) appears (Figure 3c,d). These observations are in good agreement with our hypothesis that CO preferentially adsorbs to the Na^+ ions sites and C_2H_2 to the basic framework oxygen atoms. The slight variations observed in the spectrum of adsorbed CO are probably associated with the repulsive interaction between adsorbed C_2H_2 and CO at the adjacent sites, which leads to the displacement of CO from its initial adsorption site.

The results in Figure 4 indicate that upon the temperature increase, CO desorbs from the ETS-10 and the Lewis acid sites are occupied mainly by acetylene. The weaker multiple-CO adsorption complexes are decomposed much faster than the monomeric complexes. Complete CO desorption is achieved already at −135 °C (Figure 4a). Upon the introduction of C_2H_2 at −150 °C, a substantial part of acetylene does not reach the sample and is being frozen on the cold part of the sample holder. A slight increase in temperature readily leads to the pronounced increase of the intensity of the HF band (Figure 4b) associated with the adsorption of C_2H_2 to extraframework cations that became available after desorption of CO. At room temperature, the spectra resemble closely those recorded for pure C_2H_2 adsorption as indicated in Figure 1.

Composition of ETVS-10. A series of V substituted ETS-10 samples were prepared to adjust the property of ETS-10 (XRD patterns shown in Figure S3, Supporting Information). The elemental composition of the ETVS-10 samples determined by means of ICP analysis is summarized in Table 1. With the exception of AM-6, the V content of the products is considerably lower than that in the initial gel. About 80% of the V in the initial gel is built into the framework of the samples. The K/(K+Na) molar ratio is around 0.2 for all samples.

Morphologies of ETVS-10. Figure 5 shows the SEM images of the ETVS-10 with different V content. In line with the previous results reported by Yoon et al.,[27] the as-synthesized ETS-10 crystals show a truncated bipyramidal shape with two smoother square surfaces and eight somewhat rougher isosceles trapezoidal surfaces. ETVS-10(0.1) and ETVS-10(0.3) exhibit a cubic shape with higher roughness of the surfaces and substantial crystal imperfections. ETVS-10(0.5) and ETVS-10(0.7) have similar shapes but with much smoother surfaces. The morphologies of ETVS-10(0.9) and AM-6 resemble more that of ETS-10. The crystallites in these cases are truncated bipyramids, although with less pronounced isosceles trapezoidal surfaces than in pure ETS-10. In all cases, the dimensions of crystals are several micrometers.

Local Environment Characterization of ETVS-10 by Raman Spectroscopy. The frequencies of the Raman bands related to Ti−O stretching vibrations and their fwhm are very sensitive to the presence of defect sites in the structure of ETS-10 type materials.[28−32] Previous experimental and theoretical studies pointed out that the Raman band at 724 cm^{-1} can be used as a fingerprint of the ETS-10 structure. For the materials with a higher concentration of defect sites, the frequency of this band shifts to higher wavenumber, its intensity strongly decreases, and the fwhm increases.[28−30,32−34] Similarly, the details of structural distortions in the ETS-10 lattice caused by the introduction of V ions into the −Ti−O−Ti− wires can be investigated by Raman spectroscopy.

Raman spectroscopy excited with 532 nm was employed to investigate the effect of the vanadium substitution on the local structure of lattice octahedral sites in Figure 6. The spectrum of ETS-10 is dominated by a Raman band at 724 cm^{-1}, which is the characteristic for the Ti−O stretching vibration along the

dx.doi.org/10.1021/jp305543m | J. Phys. Chem. C 2012, 116, 17124−17133

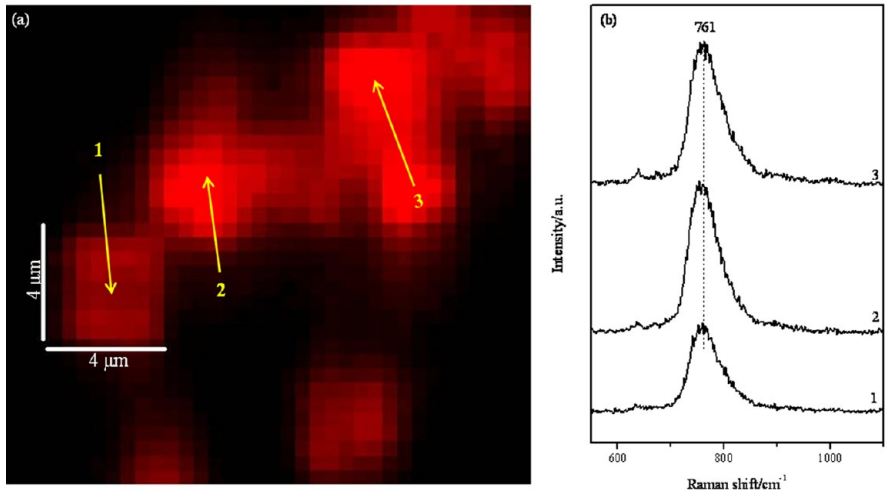

Figure 7. (a) Raman microscopy imaging of ETVS-10(0.5) (red color represents the intensity of the Raman band at 761 cm^{-1}) and (b) Raman spectra of ETVS-10(0.5) at three selected spots corresponding to the numbers in part a.

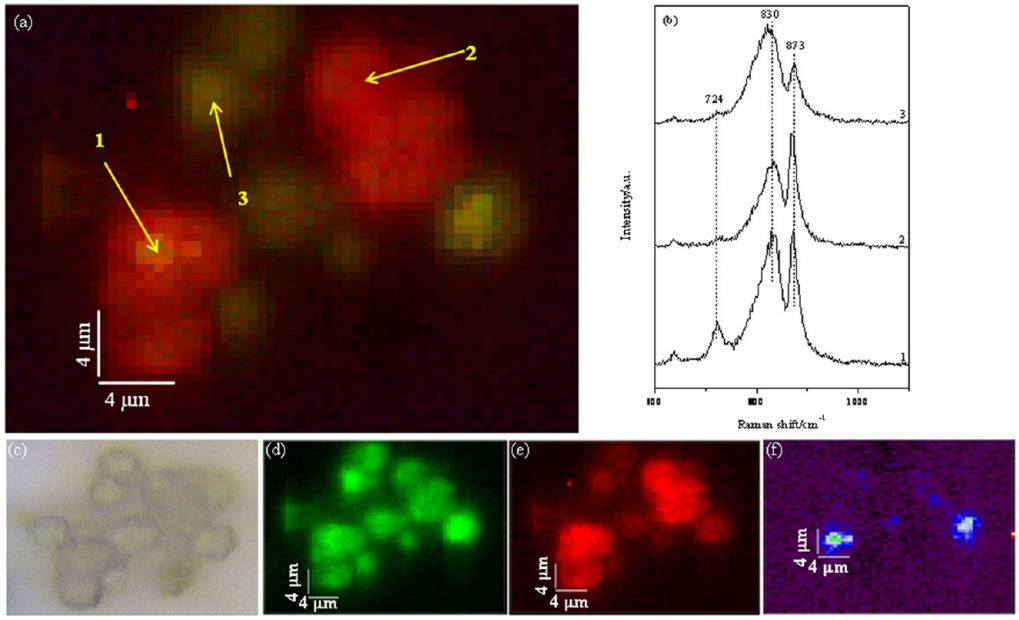

Figure 8. Raman microscopy imaging analysis of ETVS-10(0.9) with (a) Raman intensity maps (blue, green, and red represent bands at 724, 830, and 873 cm^{-1}, respectively), (b) Raman spectra at different spots corresponding to the numbers in part a, (c) optical microscopy image, (d) Raman intensity maps at 830 cm^{-1}, (e) Raman intensity maps at 873 cm^{-1}, and (f) Raman intensity maps at 724 cm^{-1}.

Ti−O−Ti wires.[28,32,35,36] Compared with ETS-10, the Raman frequency of ETVS-10(0.1) is slightly shifted to higher wavenumber (∼6 cm^{-1}) and the band has also slightly broadened. With a further increase of the V content, the Raman frequency shifts gradually to 742, 761, 777, and 830 cm^{-1} for ETVS-10(0.3), ETVS-10(0.5), ETVS-10(0.7), and ETVS-10(0.9), respectively. Simultaneously, the bands become substantially broader as compared to ETS-10. For ETVS-10(0.9), a Raman band at 873 cm^{-1} becomes apparent in the spectra. The spectrum of AM-6 shows a Raman band at 867 cm^{-1}, which is the characteristic for the V−O stretching vibration mode along the V−O−V wires.[24,37] Thus, the distinct Raman band at 873 cm^{-1} should be ascribed to the V−O stretching vibration in ETVS-10(0.9) similar to that in AM-6.[20]

In the case of ETVS-10, the introduction of lattice vanadium sites acts as "defects" by interrupting the −Ti−O−Ti− wires, and the average consecutive length of −Ti−O−Ti− will decrease due to the increasing V content. Thus, the frequency shift of the Ti species to higher wavenumber with increasing V content reveals the increasing possibility of Ti atoms meeting with V atoms via the formation of Ti−O−V in the ETVS-10. The absence of the Raman bands of the V−O stretching vibration in ETVS-10 samples with lower V content than ETVS-10(0.9) suggests that V−O species are highly isolated. However, for ETVS-10(0.9), the appearance of the Raman band at 873 cm^{-1} indicates that a number of the incorporated V atoms are in the form of aggregated −V−O−V− species. On the basis of the above discussions, a possible model is proposed in Scheme 2. The V/(V+Ti) ratios in the models correspond to the values measured by ICP in the synthesized materials. These are typically lower than the ratios in the initial gel. The distribution of Ti and V fragments is relatively homogeneous for ETVS-10(0.1), ETVS-10(0.3), ETVS-10(0.5), and ETVS-10(0.7) deduced by the single Raman band and Raman

dx.doi.org/10.1021/jp305543m | J. Phys. Chem. C 2012, 116, 17124−17133

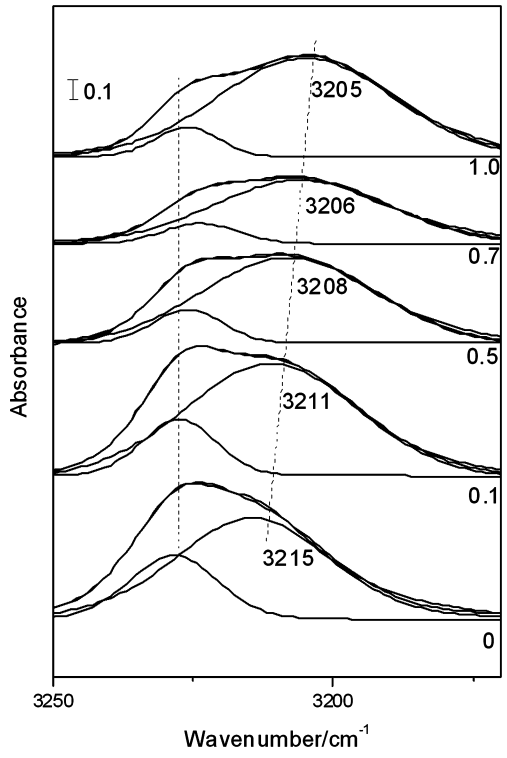

Figure 9. FTIR spectra of acetylene on ETVS-10 samples with different V content at the same equilibrium pressure of 0.5 mbar.

microscopy imaging analysis. For ETVS-10(0.9), the appearance of a band at 873 cm^{-1} indicates the formation of aggregated V−O−V species. Doren and Lobo et al. have shown that the oxidation state of the V in the chains of ETVS-10 is mainly V^{4+}, and still V^{5+} at the terminal sites of the chains.[19−22]

The Distribution of Ti and V Species of ETVS-10 by Raman Microscopy Imaging. The distribution of Ti and V species in ETVS-10(0.5) and ETVS-10(0.9) is further characterized by Raman microscopy imaging. For ETVS-10(0.5) a homogeneous distribution of the intensity of the characteristic Raman band at 761 cm^{-1} is observed (Figure 7). The Raman spectra of the individual crystallites resemble the spectrum of the powder. The imaging result proves that the single Raman band of ETVS-10 (Figure 2, 0.1 to 0.7) corresponds for the homogeneous V distribution.

In contrast, the Raman image for ETVS-10(0.9) evidence a relatively heterogeneous distribution of V and Ti. The Raman spectra of individual crystallites exhibit very different intensity ratios for the bands at 830 and 867 cm^{-1} (Figure 8b). Although the distribution of the Ti-rich regions (Raman band at 830 cm^{-1}) is quite homogeneous for all particles (Figure 8d), the distribution of V−O−V structural units is much less uniform (Figure 8e). It appears that the relative concentration of V-rich domains is higher for the larger crystals. In addition, the presence of pure ETS-10 deriving from the seeds is observed by their weak signature band at 724 cm^{-1} (Figure 8f).

A series of ETVS-10 with different framework V content are investigated by ICP, SEM, Raman spectroscopy, and Raman microscopy imaging. The Raman frequencies of the signature band for Ti wires are used as indicators for the possibility of Ti atoms meeting with V atoms in the ETVS-10. Raman spectroscopy and Raman microscopy imaging show that the distribution of Ti and V fragments is relatively homogeneous for samples with the V content below 0.9. Besides, the number of basic sites can be roughly estimated by the number of hydroxyl defects, since the location of basic sites is to the oxygen adjacent to the defects sites (Scheme 1C). The number of junctions of Ti-rich and V-rich is mainly contributed by the number of defects, since the hydroxyl defects are easily formed nearby the junctions.[20,28,38] As shown in Scheme 2, although the possibility of Ti atoms meeting with V atoms increases with increasing V content, the number of Ti atoms in the ETVS-10 crystal is decreasing at the same time. Consequently, the number of junctions first increases with increasing V content from 0 to 0.7, and decreases with increasing V content to 0.9 (Scheme 1).

Acid−Base Property of ETSV-10 Samples. FTIR spectra of acetylene adsorbed on ETVS-10 are also shown in Figure S4a−d in the Supporting Information. Qualitatively, the spectral features observed upon C_2H_2 adsorption to ETVS-10 are similar to those for ETS-10. Figure 9 compares the FTIR spectra of adsorbed acetylene on ETVS-10 with different V content at the same equilibrium pressure of 0.5 mbar. One can see that, whereas the position of the HF feature does not depend much on the V content, the LF band undergoes an increasing red shift with increasing V content. Furthermore, the ratio between the LF and HF features increases at higher V content.

Specific adsorption of acetylene to basic sites is related to the pronounced acidity of its CH bonds that can form a hydrogen bond with the lattice oxygen atoms of the framework. Depending on the basicity of the adsorption sites, the strength of the resulting hydrogen-bonded adsorption complex will vary. The formation of the hydrogen-bonded complex of acetylene weakens the CH bond and therefore causes a red shift of the corresponding CH stretching vibration (ν_{CH}). The higher the basicity of the adsorption sites is, the stronger the interaction with the CH moiety of the adsorbed molecules becomes and the larger the red shift of the CH stretching vibration is observed in the FTIR spectrum. The results presented suggest that the increasing framework V content in ETVS-10 increases the basicity of the sites. The basic sites in AM-6 are the strongest. ETVS-10 samples exhibit more moderate basicity, while the basic sites in ETS-10 are the weakest in this series of samples. Nonetheless, the basic sites in ETS-10 are much stronger than those in NaY zeolite.

A Test Reaction for Basicity. The Knoevenagel condensation (KC) is a C−C bond forming reaction, which is widely used for the synthesis of important intermediates and end products such as perfumes, pharmaceuticals, and polymers. This reaction has also been commonly used to probe the basic catalytic properties of solid catalysts.[7,25,39−42] In this way, one

Table 2. Results of the KC Reaction

sample	ETS-10	ETVS-10(0.1)	ETVS-10(0.3)	ETVS-10(0.5)	ETVS-10(0.7)	ETVS-10(0.9)	AM-6	blank
yield/%[a]	35.6	43.1	44.2	48.7	58.1	52.4	44.8	3.5

[a]No byproduct other than the KC product was obtained.

dx.doi.org/10.1021/jp305543m | J. Phys. Chem. C 2012, 116, 17124−17133

could obtain information about the total number of basic sites and the relative basic strength of different base catalysts.[42] The rate-controlling step of the condensation reaction on basic solids is the attack of the carbonyl group by the carbanion intermediate.[39,42] The results of the KC of benzaldehyde with ethyl cyanoacetate for the series of ETVS-10 samples are summarized in Table 2. With increasing V content from 0 to 0.7, the ethyl α-cyanocinnamate yield for the KC reaction between benzaldehyde and ethyl cyanoacetate gradually increases from 36% to 58%. A further increase in the V content (0.9 and 1.0) results in a pronounced decrease of the ethyl α-cyanocinnamate yield.

The effects of number and strength of the basic sites on KC reaction are considered separately. For V content of 0 to 0.1, the increase in the ECC yield is mainly due to the increase of basicity compared to the small number of junctions. For V contents in the range of 0.1 to 0.7, the increase in both intrinsic basicity and the number of basic sites leads to the further increase of catalyst activity. However, because the number of basic sites associated with the structural defects substantially decreases at the high V loadings (0.9 and 1), the ECC yield drops substantially for the respective samples, despite their higher intrinsic basicity.

4. SUMMARY

The acid and base properties of microporous titanosilicate ETS-10 were studied by coadsorption of CO and acetylene. The lattice oxygen centers adjacent to defect Ti−OH sites are identified as the basic sites. The basicity of the lattice oxygens increases with increasing V content. The strength of the basic sites increases in the order ETS-10 < ETVS-10 < AM-6.

The introduction of vanadium ions into the ETS-10 framework changes the local environment of Ti wires. The Raman frequencies of the signature band for Ti wires are used as indicators for the possibility of Ti atoms meeting with V atoms in the ETVS-10. It is roughly used to estimate the number of basic sites of ETVS-10 samples. The V distribution of ETVS-10 is homogeneous with V content lower than 0.9.

As a function of V content, the activity in the Knoevenagel condensation of benzaldehyde with ethyl cyanoacetate shows a maximum for the sample with a V/(V+Ti) of 0.7. The catalytic activity is determined both by the number and the intrinsic strength of basic sites in the ETVS-10.

■ ASSOCIATED CONTENT

Supporting Information

The 21T cluster model used for calculations; FTIR spectra of acetylene on NaY; XRD patterns of ETVS-10 with different V content; and FTIR spectra of acetylene on ETVS-10(0.1), ETVS-10(0.5), ETVS-10(0.7), and AM-6. This material is available free of charge via the Internet at http://pubs.acs.org.

■ AUTHOR INFORMATION

Corresponding Author

*Fax: (+86) 41-84694447 (C.L.). E-mail: canli@dicp.ac.cn (C.L.) and e.j.m.hensen@tue.nl (E.J.M.H.).

Notes

The authors declare no competing financial interest.

■ ACKNOWLEDGMENTS

This work was financially supported by National Basic Research Program of China (2009CB623507), National Natural Science Foundation of China (21003122), Knowledge Innovative Program of The Chinese Academy of Sciences (KGCX2-EW-310-2), and Programme Strategic Scientific Alliances between China and The Netherlands (2008DFB50130; 08-PSA-M-01). J.P.H. would like to express gratitude to the German Research Foundation DFG (postdoctoral research grant Ho4579/1-1) and NRSC-Catalysis for funding.

■ REFERENCES

(1) Philippou, A.; Naderi, M.; Rocha, J.; Anderson, M. W. *Catal. Lett.* **1998**, *53*, 221−224.
(2) Rocha, J.; Brandao, P.; de Jesus, J. D. P.; Philippou, A.; Anderson, M. W. *Chem. Commun.* **1999**, 471−472.
(3) Brandao, P.; Philippou, A.; Valente, A.; Rocha, J.; Anderson, M. *Phys. Chem. Chem. Phys.* **2001**, *3*, 1773−1777.
(4) Valente, A.; Lin, Z.; Brandao, P.; Portugal, I.; Anderson, M.; Rocha, J. *J. Catal.* **2001**, *200*, 99−105.
(5) Philippou, A.; Anderson, M. W. *J. Catal.* **2000**, *189*, 395−400.
(6) Ono, Y. *J. Catal.* **2003**, *216*, 406−415.
(7) Lima, S.; Dias, A. S.; Lin, Z.; Brandao, P.; Ferreira, P.; Pillinger, M.; Rocha, J.; Calvino-Casilda, V.; Valente, A. A. *Appl. Catal., A* **2008**, *339*, 21−27.
(8) Lercher, J. A.; Grundling, C.; EderMirth, G. *Catal. Today* **1996**, *27*, 353−376.
(9) Anderson, M. W.; Terasaki, O.; Ohsuna, T.; Philippou, A.; Mackay, S. P.; Ferreira, A.; Rocha, J.; Lidin, S. *Nature* **1994**, *367*, 347−351.
(10) Knozinger, H.; Huber, S. *J. Chem. Soc., Faraday Trans.* **1998**, *94*, 2047−2059.
(11) Lavalley, J. C. *Catal. Today* **1996**, *27*, 377−401.
(12) Schoonheydt, R.; Geerlings, P.; Pidko, E.; Santen, R. A. *J. Mater. Chem.* **2012**, DOI: 10.1039/C2JM31366A.
(13) Hadjiivanov, K. I.; Vayssilov, G. N. *Adv. Catal.* **2002**, *47*, 307−511.
(14) Zecchina, A.; Bordiga, S.; Spoto, G.; Scarano, D.; Petrini, G.; Leofanti, G.; Padovan, M.; Arean, C. O. *J. Chem. Soc., Faraday Trans.* **1992**, *88*, 2959−2969.
(15) Rocha, J.; Lin, Z.; Ferreira, A.; Anderson, M. W. *J. Chem. Soc., Chem. Commun.* **1995**, 867−868.
(16) Brandao, P.; Valente, A. A.; Rocha, J.; Anderson, M. W. *Stud. Surf. Sci. Catal.* **2002**, *142*, 327−334.
(17) Eldewik, A.; Howe, R. F. *Microporous Mesoporous Mater.* **2001**, *48*, 65−71.
(18) Anderson, M. W.; Rocha, J.; Lin, Z.; Philippou, A.; Orion, I.; Ferreira, A. *Microporous Mater.* **1996**, *6*, 195−201.
(19) Shough, A. M.; Lobo, R. F.; Doren, D. J. *Phys. Chem. Chem. Phys.* **2007**, *9*, 5096−5104.
(20) Nash, M. J.; Rykov, S.; Lobo, R. F.; Doren, D. J.; Wachs, I. *J. Phys. Chem. C* **2007**, *111*, 7029−7037.
(21) Shough, A. M.; Doren, D. J.; Nash, M.; Loho, R. F. *J. Phys. Chem. C* **2007**, *111*, 1776−1782.
(22) Ooms, K.; Polenova, T.; Shough, A. M.; Doren, D. J.; Nash, M. J.; Lobo, R. F. *J. Phys. Chem. C* **2009**, *113*, 10477−10484.
(23) Shough, A. M.; Doren, D. J.; Ogunnaike, B. *Chem. Mater.* **2009**, *21*, 1232−1241.
(24) Rocha, J.; Brandao, P.; Lin, Z.; Anderson, M. W.; Alfredsson, V.; Terasaki, O. *Angew. Chem., Int. Ed. Engl.* **1997**, *36*, 100−102.
(25) Goa, Y.; Wu, P.; Tatsumi, T. *J. Catal.* **2004**, *224*, 107−114.
(26) Kishima, M.; Okubo, T. *J. Phys. Chem. B* **2003**, *107*, 8462−8468.
(27) Jeong, N. C.; Lee, M. H.; Yoon, K. B. *Angew. Chem., Int. Ed.* **2007**, *46*, 5868−5872.
(28) Southon, P. D.; Howe, R. F. *Chem. Mater.* **2002**, *14*, 4209−4218.
(29) Guo, M. L.; Feng, Z. C.; Li, G. N.; Hofmann, J. P.; Pidko, E. A.; Magusin, P. C. M. M.; Guo, Q.; Weckhuysen, B. M.; Hensen, E. J. M.; Li, C. *Chem.—Eur. J.* **2012**, DOI: 10.1002/chem.201200875.
(30) Pavel, C. C.; Park, S. H.; Dreier, A.; Tesche, B.; Schmidt, W. *Chem. Mater.* **2006**, *18*, 3813−3820.

(31) Pavel, C. C.; Zibrowius, B.; Loffler, E.; Schmidt, W. *Phys. Chem. Chem. Phys.* **2007**, *9*, 3440−3446.
(32) Xamena, F. X. L. I.; Damin, A.; Bordiga, S.; Zecchina, A. *Chem. Commun.* **2003**, 1514−1515.
(33) Yilmaz, B.; Warzywoda, J.; Sacco, A. *Nanotechnology* **2006**, *17*, 4092−4099.
(34) Lv, L.; Zhou, J. K.; Su, F.; Zhao, X. S. *J. Phys. Chem. C* **2007**, *111*, 773−778.
(35) Damin, A.; Xamena, F. X. L.; Lamberti, C.; Civalleri, B.; Zicovich-Wilson, C. M.; Zecchina, A. *J. Phys. Chem. B* **2004**, *108*, 1328−1336.
(36) Su, Y.; Balmer, M. L.; Bunker, B. C. *J. Phys. Chem. B* **2000**, *104*, 8160−8169.
(37) Yeates, R. M.; Murdoch, M. J.; Southon, P. D.; Mclaughlin, A. C.; Howe, R. F.; Bonino, F.; Bordiga, S.; Damin, A. *Dalton Trans.* **2009**, 8025−8032.
(38) Anderson, M. W.; Agger, J. R.; Hanif, N.; Terasaki, O. *Microporous Mesoporous Mater.* **2001**, *48*, 1−9.
(39) Corma, A.; Fornes, V.; Martinaranda, R. M.; Garcia, H.; Primo, J. *Appl. Catal.* **1990**, *59*, 237−248.
(40) Corma, A.; Fornes, V.; Martinaranda, R. M.; Rey, F. *J. Catal.* **1992**, *134*, 58−65.
(41) Lopezgonzalez, J. D.; Lopezpeinado, A.; Martinaranda, R. M.; Rojascervantes, M. L. *Carbon* **1993**, *31*, 1231−1236.
(42) Climent, M. J.; Corma, A.; Iborra, S.; Velty, A. *J. Mol. Catal. A: Chem.* **2002**, *182*, 327−342.